Asian Journal of Physics
Vol. 31, No 7 (2022) 723-730
Available on: www.asianjournalofphysics.com

ap

New family of Jacobi-Fourier aberrations for wavefront coding

E Acosta[1], E González Amador[1,2], A Padilla[2] and J Arines[1]

[1]*Department of Applied Physics, Faculty of Physics,*
University of Santiago de Compostela, 15782 Santiago de Compostela, Spain

[2]*Department of Optics, Faculty of Optical Computing,*
University Politécnica de Tulancingo, 46629 Tulancingo Hidalgo, México

Dedicated to Prof Maria J Yzuel

Wavefront coding is a hybrid optical-digital imaging system technique which generates aberrations using a phase mask or a phase generating device at the exit pupil of an optical system in order to extend its depth of focus. The optical system generates an intermediate low-quality image blurred by the aberrations of the added phase and, a sharp final image is obtained by a deconvolution process involving the optical transfer function (OTF) of the whole optical system at the image plane. Many shapes for the added phase have been proposed and they differ among each other in the quality of the decoded images within a given depth of focus as well as the noise and artifacts transferred to the postprocessed image. In this work, we will present a new set of phase masks based on Jacobi-Fourier polynomials and show the advantages and disadvantages comparing with the commonly used trefoil aberration.

Keywords: Wavefront coding, Jacobi-Fourier polynomials, Trefoil aberration, Fourier transform.

1 Introduction

Wavefront coding (WFC) is a hybrid optical-computational technique using a phase modulating device (PM), as a deformable mirror, a liquid crystal device or a phase mask at the exit pupil of an imaging system encoding a controlled amount of aberration in order to extend the depth of focus (DOF) of the imaging system. The amount of aberration generated by the PM makes the Point Spread Function (PSF) and the Optical Transfer Function of the system (OTF) nearly invariant to defocus as well as to misfocus related aberration. This technique was proposed by Dowsky and Kathey [1] and it was successfully used in many applications as iris recognition [2], infrared imaging [3], fluorescent microscopy [4], ophthalmoscopy [5,6] among others. The great advantage of WFC is to increase the performance of an optical systems by increasing its DOF and at the same time it allows to reduce its cost and complexity [7].

In a previous work [5], we presented a set of aberrations in the shape of a subset of Jacobi-Fourier polynomials to overcome some issues that the trefoil aberration, generates, as noise propagation and artifacts in the decoded images. In this work, we will expand the subset to optimize the results in order to get the better ecoded images.

2 Background: Cubic and related masks

The first PM used to demonstrate the ability to increase the DOF of hybrid optical systems was a cubic mask in the shape [1]

$$S(x, y) = \alpha (x^3 + y^3), \tag{1}$$

Corresponding author
e mail: eva.acosta@usc.es (E Acosta); enrique.amador@upt.edu.mx (E González Amador)

where, α represents the strength of the PM, i.e., the half of the peak to valley (P-V) aberration generated by the PM. The key to increase the DOF is to get an OTF nearly invariant to defocus at the same time it has no zeroes and, therefore, deconvolution is not an ill posed problem. Cubic masks accomplished both conditions. Based on these results, other masks, with slight variations of the cubic masks, have been proposed: root square [8], sinusoidal [9] the exponential [10], the tangential [11], the logarithmic [12] and the rational [13] can be cited among many others.

The common feature of all these masks is the typical L shaped PSF. Nevertheless, there are differences in the corresponding OTF's what will translate into different amount of noise and artifacts of the decoded images. Next quantitative step in the shape of the PM was found by Prasad *et al* [14] and they found that trefoil PM performs much better than the cubic one. Trefoil aberration does not change the order of the polynomial defining the shape, i.e., the radial coordinate is still r^3 but the angular dependence changes as shown in Table 1:

Table 1. Phase masks

	Cubic	Trefoil
XY Coordinates	$x^3 + y^3$	$x(x^2 - 3y^2)$
Polar Coordinates	$r^3(\cos^3\theta + \sin^3\theta)$	$r^3 \cos 3\theta$

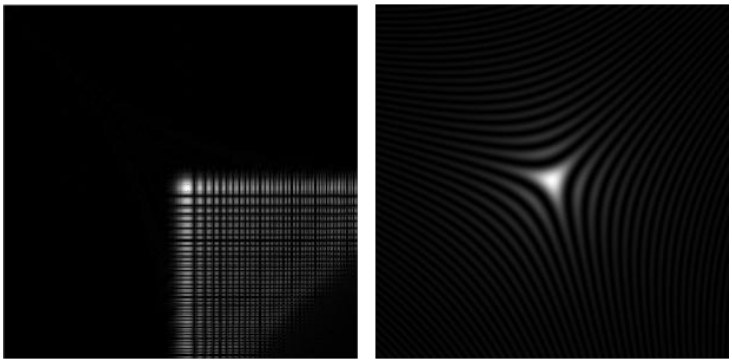

Fig 1. PSF of cubic PM (left) and trefoil PM (right).

3 Jacobi-Fourier phase masks

Recently, Nhu *et al* [8] demonstrated that a smooth shape of the PM at the central part of the pupil and a rapid variation at the periphery are important features for a PM to have a good performance. Based on these results, we proposed the use of a subset of JFP to improve the performance of a trefoil PM [15]. These JFP have the shape

$$JFP(p, m, r, \theta) \propto J_0(p, p, r)\cos(m\theta), \tag{2}$$

where, $J_0(p, p, r)$ is the Jacobi polynomial $J_n(p, q, r)$ [16] with $n = 0$, $p = q$, being p an integer and $m = 3$. The radial dependence of the PMs is shown in Table 2.

It can be seen that for $p = 7$ we obtain the trefoil aberration. In references [15,17] we showed that the proper choice of the p value is a trade-off among signal to noise ratio, desired depth of focus and presence of artifacts for a given $f/\#$ of the optical system: In general, we found that small values of p are related with the presence of artifacts and noise enhancement but large values of p shorten the depth of focus.

Table 2. Radial dependence of JFP PM

p	*Radial dependence*
6	$r^{5/2}$
7	r^{3}
8	$r^{5/2}$
9	r^{4}
10	$r^{9/2}$

In this work, in order to optimize the design of JFP PMs, we will consider p to be a rational number multiple of $N/2$, being N an integer. This provides an extra degree of freedom to optimize the performance of WFC optical systems.

In order to illustrate the work, we will show numerical simulations for an optical system with PMs whose shape has radial dependence between r^3 and r^4 as in Table 3.

Table 3. Radial dependence of JFP PM in this work#

p	*Radial dependence*
14/2	r^{3}
15/2	$r^{13/4}$
16/2	$r^{14/4}$
17/2	$r^{15/4}$
18/2	r^{4}

4 Numerical Simulations

In this section, we will show and analyze the performance of the five JFP PMs in Table 2. We consider an optical system with $f/2.5$ and a wavelength of $\lambda = 632$ nm. This optical system has been already analyzed in ref [15] for integer p values between 6 and 10. For a value of the strength of $\alpha = 50$ λ and considering both noiseless and noisy cases, we found that p values of 6, 7 and 8 performed better. In this work, we will consider the same noise values as those provided in ref [15], but we will study the performance of JFP PMs with p value between 7 and 9. Figure 2 shows 2D contour maps of the different PMs where radius of pupil has been normalized to unity. It can be observed that as p increases the central region becomes flatter.

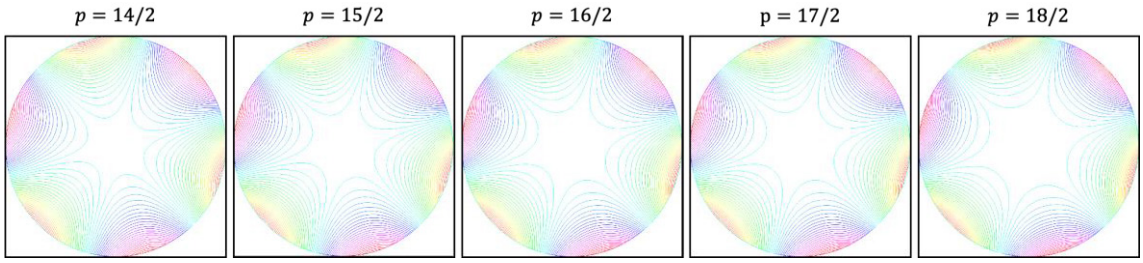

Fig 2. 2D colormaps.

Performance at four different recording planes with an amount of defocus, W_{20}, of 1 λ, 3 λ, 5 λ and 7 λ will be studied. Here,

$$W_{20} = \frac{\Delta z}{8\lambda (f/\#)^2} \tag{3}$$

where, Δz is the distance between the paraxial focal plane and the recording plane.

The OTFs were computed as the inverse discrete Fourier Transform of the PSF [18]. FFT evaluations were performed by routines provided by Matlab and sampling of the pupil plane on a grid of 4096 × 4096 and a pixel size at the image plane of 0.79 μm in order to work in the limit of the Nyquist theorem [18,19] and avoid extra aliasing due to undersampling of the phase at the pupil of the optical system [20].

In Fig 3, we plot the optical Modulated Transfer Functions, MTF, for the different defocus values, $MTF(W_{20})$.

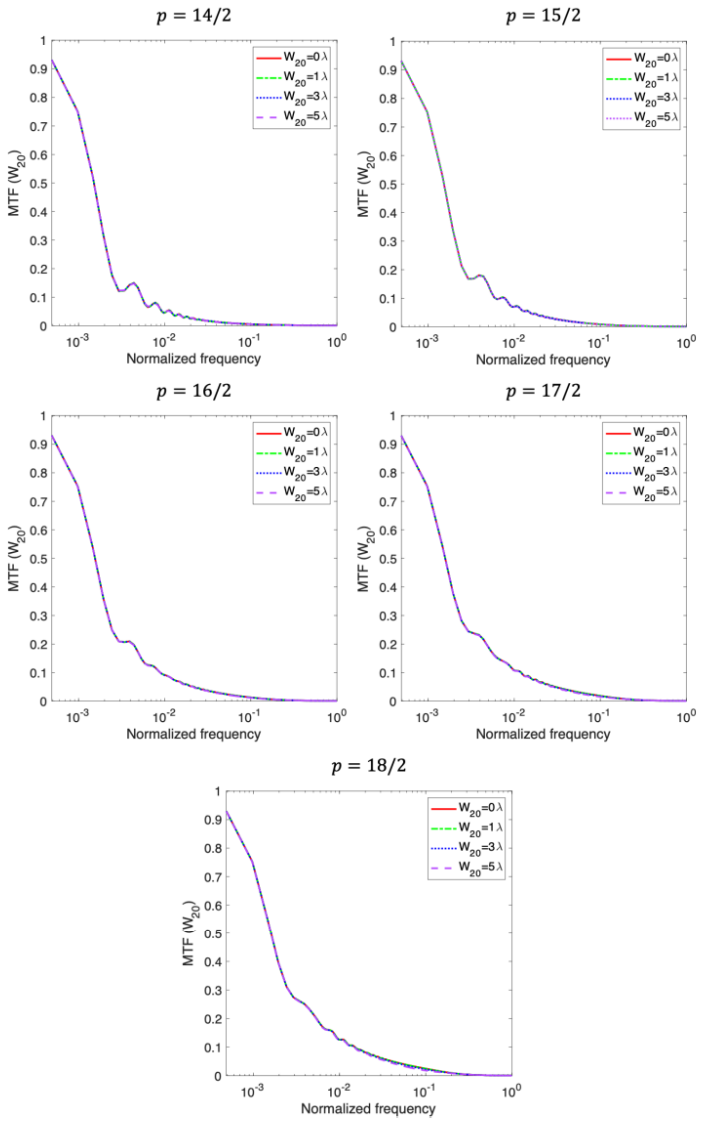

Fig 3. $MTF(W_{20})$ corresponding to the different PMs labeled by p and for different defocus values.

We can observe that in all cases none of the $MTF(W_{20})$ has zeroes, and therefore deconvolution is not an ill posed problem. As p increases the amplitude of the $MTF(W_{20})$. increases, and this will have an impact on the signal to noise ratio of the coded images, and therefore, on the quality of the decoded

images. On the other hand, as p increases, there is a slight loss of invariance in the defocus range. All $MTF(W_{20})$ show ripples or oscillations for low frequencies. The number and height of oscillations decrease as p increases. This behaviour is more evident in Fig 4, where we plot the system MTF, $MTF_{system}(W_{20})$, defined as:

$$MTF_{system}(W_{20}) = \frac{MTF(W_{20})}{MTF(0)} \tag{4}$$

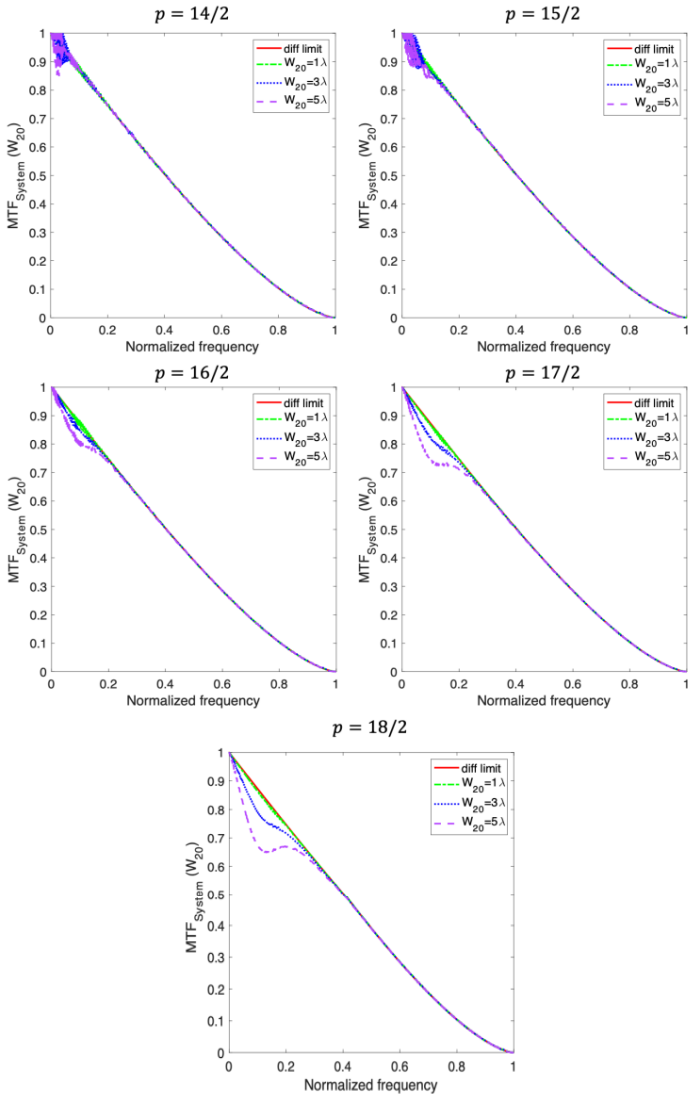

Fig 4. $MTF_{system}(W_{20})$ corresponding to the different PM labeled by p and for different defocus values.

Finally, in Figs 5 and 6, we show decoded images for the different PMs and the different defocus values. Figure 5 represents the noiseless case and Fig 6 shows the noisy one obtained by adding to the intermediate images random Gaussian noise with zero mean and two different values of standard deviation: 0.2% and 1%, of the maximum value of the gray level of the optically coded image.

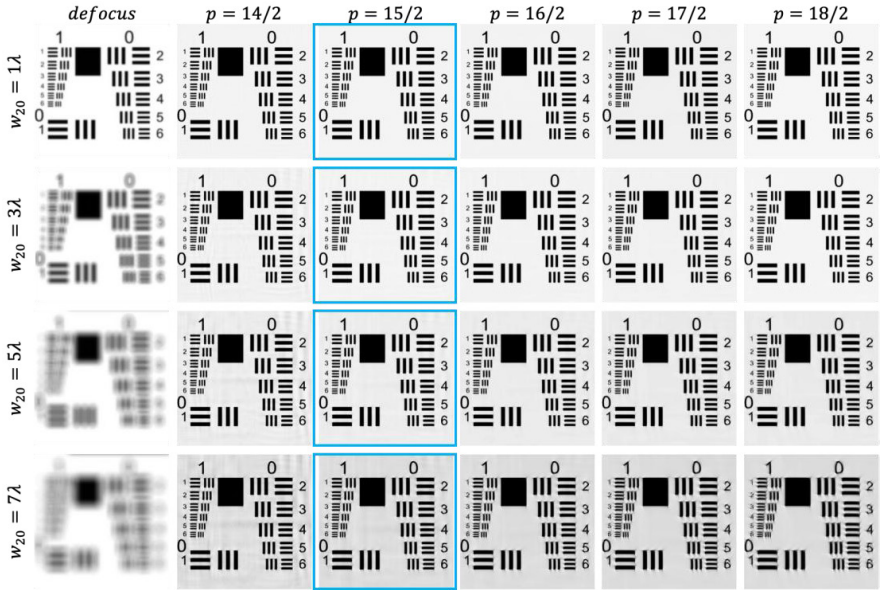

Fig 5. Decoded images with the different PM and different defocus values from intermediate free of noise images. First column shows the defocused images of the optical system without PM.

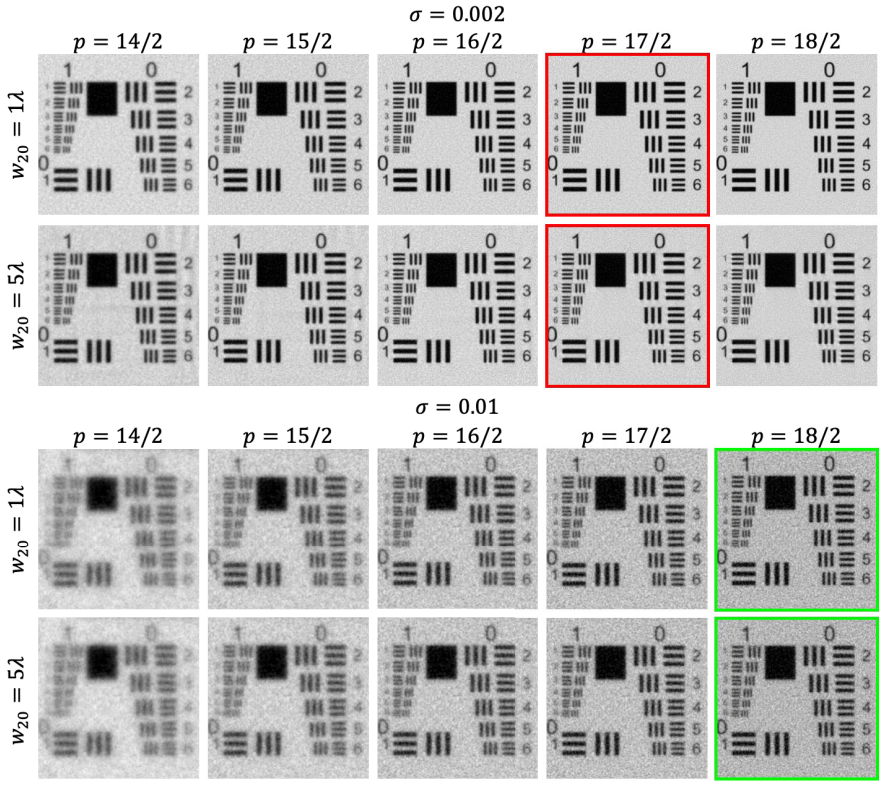

Fig 6. Decoded images with the different PM and two different defocus values from intermediate images with 0.2% added noise (upper rows) and 1% added noise (lower rows).

5 Discussion

From Fig 5 (noiseless case), we can observe that artifacts (replicas) appear for small values of p and they become more visible as defocus increases. This is due to the ripples that *MTFs* show for low frequencies, but resolution is better than that of larger p values because *MTFs* are practically invariant. On the other hand, for large values of p, images suffer distortion and artifacts at the edges of the bars. This is due to the small loss of invariance of the *MTF*s with both $\boldsymbol{p}$ and defocus. Nevertheless, there are no artifacts in the shape of replicas because *MTFs* show no oscillations for low frequencies. Here, we could say that $p = 15/2$ (blue squares) provides the best trade-off artifacts-DOF, better than the proposed $p = 16/2$ in ref [15].

From Fig 6, we can observe that noise minimizes artifacts as well as distortion for small values of p and minimizes artifacts for the large ones. Nevertheless, noise propagation is strong for small p values what makes the images loose resolution and DOF. The higher the noise, the larger should be p. Here, we could say that $p = 18/2$ (green squares) provides the best trade off artifacts-DOF-noise, as proposed in ref [15] for 1% noise, but $p = 17/2$ (red squares) performs better than $p = 16/2$ for 0.2% noise.

6 Conclusions

In this work, we explore the use of an extended subset of Jacobi-Fourier phase masks to both optimize image quality and extend the depth of focus in an WFC optical imaging system. For the radial part, we used Jacobi polynomials $J_0(p, p, r)$, being $p = N/2$, N an integer. For the azimuthal dependence, we used $\cos(3\theta)$ to compare with the Trefoil Phase Mask ($p = 14/2$).

The optical system we use to simulate the performance of these masks is an optical system with $f/\# = 2.50$ and $\lambda = 632$ nm. Results are shown for a PM strength $\alpha = 50\lambda$ that provides depth of focus up to 7λ in the best scenario.

We found that small values of p yield decoded images with artifacts, the smaller the p value the higher the amount of artifacts and the larger DOF when noise is zero or neglectable. For higher level of noise, higher values of p perform better, i.e. the higher the noise the higher the p value performs better. These results agree with the analysis of the *MTF* plots. For small values of p, the plots show ripples which result in the presence of artifacts in the decoded images. Larger p value give rise to softer curves and hence fewer artifacts. The higher the p value, the higher the *MTF* values and hence the best behavior in the presence of noise. However, invariance is gradually lost as p increases, which implies that as p increases, the depth of focus decreases. In other words, the proper choice of the p value is a trade-off among signal to noise ratio, desired depth of focus and presence of artifacts for a given $f/\#$ and this choice can be optimized if we make use of the set of JFP PM described in this work because we are adding a degree of freedom to the formula of JFP PMs proposed in ref [15].

References

1. Dowski E R, Cathey W T, Extended depth of field through wave-front coding, *Appl Opt*, 34(1995)1859–1866.
2. Barwick, D S, Increasing the information acquisition volume in iris recognition systems, *Appl Opt*, 47(2008)4684–4691.
3. Muyo G, Singh A, Andersson M, Huckridge D, Wood A, Harvey A R, Infrared imaging with a wavefront-coded singlet lens, *Opt Express*,17(2009)21118–21123.
4. Arnison M R, Cogswell C J, Sheppard C J, Török P, Wavefront coding fluorescence microscopy using high aperture lenses, in Optical Imaging and Microscopy: Techniques and Advanced Systems, (Eds) Török P, Kao F.-J, (Springer), 2003, pp 143–165.
5. Acosta E, Olvera-Angeles M, González-Amador E, Sasian J, Schwiegerling J, Arines J, Wavefront coding with Jacobi–Fourier phase masks for retinal imaging, *Appl Opt*, 59(2020)G234-G238.

6. Acosta E, Arines J, Optical-digital System Invariant to eye aberrations for retinal imaging, *Investig Ophthalmol Vis Sci*, 53(2012)3098–3098.
7. Kubala K, Dowski E, Cathey WT, Reducing complexity in computational imaging systems, *Opt Express*, 11(2003)2102–2108.
8. Nhu V, Fan Z, Minh N P, Chen S, Optimized square-root phase mask to generate defocus-invariant modulation transfer function in hybrid imaging systems, *Opt Eng*, 54(2015)035103; doi.org/10.1117/1.OE.54.3.035103.
9. Zhao H, Li Y, Analytical and experimental demonstration of depth of field extension for incoherent imaging system with a standard sinusoidal phase mask, *Chin Opt Lett*, 10(2012)031101; doi: 10.3788/COL201210.031101.
10. Yang Q, Liu L, Sun J, Optimized phase pupil masks for extended depth of field, *Opt Commun*, 272(2007)56–66.
11. Chen S, Fan Z, Optimized asymmetrical tangent phase mask to obtain defocus invariant modulation transfer function in incoherent imaging systems, *Opt Lett*, 39(2014)2171–2174.
12. Zhao H, Li Y, Performance of an improved logarithmic phase mask with optimized parameters in a wavefront-coding system, *Appl Opt*, 49(2010)229–238.
13. Zhou F, Li G, Zhang H, Wang D, Rational phase mask to extend the depth of field in optical-digital hybrid imaging systems, *Opt Lett*, 34(2009)380–382.
14. Prasad S, Torgersen T C, Pauca V P, Plemmons R J, van der Gracht J, Engineering the pupil phase to improve image quality, In Visual Information Processing XII. Proc SPIE, 5108(2003)1-13; doi.org/10.1117/12.487572.
15. González-Amador E, Padilla-Vivanco A, Toxqui-Quitl C, Arines J, Acosta E, Jacobi–Fourier phase mask for wavefront coding, *Opt Lasers Eng*, 126(2020)105880; doi.org/10.1016/j.optlaseng.2019.105880.
16. Camacho-Bello C, Toxqui-Quitl C, Padilla-Vivanco A, Báez-Rojas J J, High-precision and fast computation of Jacobi–Fourier moments for image description, *J Opt Soc Am*, 31(2014)124–134.
17. González-Amador E, Padilla-Vivanco A, Arines J, Olvera-Angeles M, Acosta E, Choice of Jacobi–Fourier phase masks for wavefront coding under different f-number, *Jpn J Appl Phys*, 59(2020)SOOD04; doi.org/10.35848/1347-4065/ab9652.
18. Voelz D G, Computational Fourier optics: a MATLAB tutorial, (SPIE press) 2011.
19. Zhou M, Alfadhl Y, Chen X, Optimal spatial sampling criterion in a 2D THz holographic imaging system, *IEEE Access*, 6(2018)8173–8177.
20. Acosta E, González-Amador E, Arines J, Optimizing sampling and padding at the pupil plane for light propagation simulations based in Fourier Transforms for wavefront coding, *Asian J Phys*, 30(2021)1235–1241.

[*Received*: 02.04.2022; *accepted*: 01.05.2022]